On the natural stabilization of convection dominated problems using high order Bubnov–Galerkin finite elements

Q. Cai [a,*], S. Kollmannsberger [a], E. Sala-Lardies [b], A. Huerta [b], E. Rank [a]

[a] Computation in Engineering, Faculty of Civil Engineering and Geodesy, Technische Universität München, Arcisstr. 21, D-80290 München, Germany

[b] Laboratori de Càlcul Numèric (LaCàN), Department de Matemàtica Aplicada III, Universitat Politècnica de Catalunya. Jordi Girona 1, E-08034 Barcelona, Spain

ARTICLE INFO

ABSTRACT

In the case of dominating convection, standard Bubnov–Galerkin finite elements are known to deliver oscillating discrete solutions for the convection–diffusion equation. This paper demonstrates that increasing the polynomial degree (p-extension) limits these artificial numerical oscillations. This is contrary to a widespread notion that an increase of the polynomial degree destabilizes the discrete solution. This treatise also provides explicit expressions as to which polynomial degree is sufficiently high to obtain stable solutions for a given Péclet number at the nodes of a mesh.

© 2013 Elsevier Ltd. All rights reserved.

1. Introduction

Many stabilized finite element methods have been proposed in literature which can effectively reduce or even eliminate numerical oscillations in convection-dominated convection–diffusion problems. A very popular approach is the streamline upwind Petrov–Galerkin method (SUPG) [1,2]. It achieves stability by adding additional artificial diffusion which needs to be modeled explicitly. Alternatively, the local projection stabilization (LPS) [3–5] suppresses numerical oscillations without refining the mesh or enriching the finite element space. Instead, locally constructed stabilization parameters must be chosen. Other methods, such as the orthogonal subgrid scale (OSS) [6], the Galerkin least-squares (GLS) [7] and the variational multi-scale method (VMS) [8–10] provide a wealth of cures for the curse of artificial oscillations in convection-dominated problems. These methods are usually applied to low order finite elements. A review of available approaches is given in [11], for instance. For a review focusing on classic high order methods see [12], among others.

In the context of high-order accuracy, which is of particular interest within the scope of this paper, novel approaches such as the nodal discontinuous Galerkin method [13] or a discontinuous Petrov–Galerkin method [14] provide computationally attractive alternatives. The latter was extended in [15,16] and utilizes a space of discontinuous test functions tailored for stability. It provides optimal error estimates with respect to the element size h and polynomial degree p in a given norm for discrete solutions on a general mesh and is thus highly suitable for adaptivity [17].

In the parameter-free stabilized finite element method, which was developed by Bochev and Peterson [18], the relationship between nodal Galerkin diffusive fluxes and diffusion equations in one dimension on the mesh edges is extended to the advection–diffusion case by solving simplified, one-dimensional versions of the governing equations on the edges. This method is first-order accurate but less dissipative than the classical artificial diffusion approach. Extensions to higher polynomial orders are promised but they have yet to be published.

---

* Corresponding author.
  E-mail addresses: quanji.cai@tum.de, cai@bv.tum.de (Q. Cai), kollmannsberger@bv.tum.de (S. Kollmannsberger), esther.sala-lardies@upc.edu (E. Sala-Lardies), antonio.huerta@upc.edu (A. Huerta), rank@bv.tum.de (E. Rank).

An interesting further option for a stable discretization of the steady convection–diffusion equation is provided by the enforcement of constraints in a variational multiscale analysis [19]. The method decomposes the solution into a sum of fine and coarse scale components. The fine scale is determined analytically in terms of the coarse scale component and the coarse scale is then solved for numerically. The method defines the decomposition procedure through a constrained optimization problem and allows for an enforcement of the maximum principle.

Another alternative is the Residual-Free Bubble method, as proposed by Brezzi and Russo [20–22] for convection–diffusion problems. It has also been analyzed for a spectral Legendre discretization for advection–diffusion problems in [23]. Polynomial shape functions within an element are enriched by residual-free bubble functions. The effect of the residual-free bubbles on the formulation is to add stability through jump terms measuring the differences in the streamline direction of the bilinear (or linear) values of the solution [24–26]. Interestingly, the Residual-Free Bubble method and the variational multiscale method (VMS) cited above are conceptionally equivalent. This was proven in [27].

For convection–diffusion problems discretized by high order finite element methods (also referred to as p-FEM), Tobiska [28] developed a new stabilized technique by combining the p-FEM and the VMS approach. Roos et al. [29] discovered that higher order polynomial degrees behaved better in numerical experiments than low order elements. [30] looks at the high order finite element method in conjunction with SUPG and shock-capturing stabilization.

All methods mentioned above provide the means for an effective stabilization of convection-dominated problems which are also applicable, or even specifically designed for their use in high-order discretizations. Nevertheless, the high order Bubnov–Galerkin method itself, *without* extra stabilization, already exhibits a stabilizing effect, as will be shown in this paper.

Merely increasing the polynomial degree of the shape functions is, of course, not necessarily as efficient as schemes directly designed for the job of stabilizing convection–diffusion problems. We do show, however, that a higher order might already provide sufficient stability for convection-dominated problems in the case of low or moderate *Péclet* numbers, as they appear in flows through porous media, for instance. In these cases, the scheme may also easily outperform low order stabilized methods, thanks to its high accuracy and, in many cases, exponential rate of convergence. In this context, it is still necessary to know from which polynomial degree a Bubnov–Galerkin discretization remains stable for a given *Péclet* number. Estimates have been published in [31–33], for example. The current paper provides sharp stability bounds.

The layout of the paper is as follows: We start by introducing the problem in the form of a one-dimensional, convection–diffusion equation with constant coefficients in Section 2. Then, Section 3 recalls the Bubnov–Galerkin discretization with linear elements and quantifies the truncation error of this low order scheme. The truncation error appears in the diffusion term and is a decisive factor as it is directly related to the artificially generated, numerical oscillations in convection-dominated problems. Up to this point, this analysis is familiar from descriptions in [34], for instance. Section 4 shows, however, that a straightforward p-FEM extension naturally decreases this truncation error. The high order Bubnov–Galerkin method, therefore, gradually compensates for the lost diffusivity of low order schemes as it approaches the quantified diffusivity derived in Section 3. Section 5 derives which polynomial degree is sufficiently high to completely eliminate numerical oscillations at the nodes. To validate the mathematical analysis, one- and two-dimensional numerical examples are studied in Section 6. Section 7 then concludes the article.

2. Problem statement

This paper investigates the following one-dimensional steady convection–diffusion transport problem in $\Omega = (0, 1)$:

$$ac'(x) - vc''(x) = f. \tag{1}$$

Here, c is the scalar unknown (concentration, in this paper), a is the convection velocity, v is the diffusivity of the fluid and f is the source term. Throughout this paper it is assumed that these three coefficients have constant values across the whole domain. For the source term $f = 1$ and the Dirichlet boundary condition $c(x = 0) = c(x = 1) = 0$, the analytical solution reads:

$$c(x) = \frac{1}{a} \left(x - \frac{1 - e^{\frac{ax}{v}}}{1 - e^{\frac{a}{v}}} \right). \tag{2}$$

We discuss the discretization on an equidistant mesh with the size h. At this point, it is useful to introduce the mesh *Péclet* number *Pe* [34] defined in Eq. (3) to characterize the local dominance of convection and diffusion from a numerical perspective.

$$Pe = \frac{ah}{2v}. \tag{3}$$

It is well known that the numerical solution of Eq. (1) is stable for the problem with piecewise linear elements if *Pe* is not greater than 1. The straightforward application of the Bubnov–Galerkin discretization leads to the corresponding weak form of Eq. (1).

$$\begin{cases} \int_{\Omega} (ac'w + c'vw')d\Omega = \int_{\Omega} fwd\Omega & \text{on } \Omega = \{x|0 < x < 1\} \\ c = 0 & \text{at } x = 0 \\ c = 0 & \text{at } x = 1 \end{cases} \tag{4}$$

where w is a test function vanishing at the boundaries i.e. $w, c \in H_0^1(\Omega)$. The scalar functions c and w are both discretized and approximated by the same shape functions N_i. This leads to Eq. (5) which contains the convection matrix **C**, diffusion matrix **K** and force vector **f**.

$$(\mathbf{C} + \mathbf{K})\mathbf{c} = \mathbf{f}. \tag{5}$$

The matrices **C** and **K** are of dimension $n \times n$, n denoting the number of unknown coefficients. **C** and **K** are obtained by assembling the element convection matrix $\mathbf{C}^e$ and element diffusion matrix $\mathbf{K}^e$, respectively.

In the one-dimensional example of Eq. (1), $\mathbf{C}^e$, $\mathbf{K}^e$ and $\mathbf{f}^e$ are defined as:

$$
\begin{aligned}
C_{ij}^e &= \int_0^1 a N_i N_{j,x} dx \\
K_{ij}^e &= \int_0^1 \nu N_{i,x} N_{j,x} dx \\
f_i^e &= \int_0^1 f N_i dx.
\end{aligned}
\tag{6}
$$

The Bubnov–Galerkin discretization is known to be optimal for elliptic problems. However, when the convection flux becomes dominant, i.e. as Pe grows, the accuracy of the previously obtained solution declines for a fixed polynomial degree. The next section explains the effect of Pe on the accuracy of the nodal solution.

3. The Bubnov–Galerkin method with linear elements

We now look at the problem set out in Eq. (1) with two adjacent elements $[x_{j-1}, x_j]$ and $[x_j, x_{j+1}]$, as depicted in Fig. 1, where the node x_j is shared by two elements. For the sake of simplicity, we apply the source term $f = 1$ and discretize the geometry using a uniform mesh with element length h. The shape functions of a linear element are given by [35]

$$N_1(\xi) = \frac{1-\xi}{2} \tag{7}$$

$$N_2(\xi) = \frac{1+\xi}{2} \tag{8}$$

where ξ is the normalized local coordinate. Setting $\Omega_j^e = [x_j, x_{j+1}] \in [-1, 1]$ and applying the transformation between local and global coordinates, we obtain the following convective and diffusive matrix as well as the force vector [34] for each element.

$$C^e = a \int_{\Omega^e} \begin{pmatrix} N_1 \dfrac{\partial N_1}{\partial x} & N_1 \dfrac{\partial N_2}{\partial x} \\ N_2 \dfrac{\partial N_1}{\partial x} & N_2 \dfrac{\partial N_2}{\partial x} \end{pmatrix} dx = \frac{a}{2} \begin{pmatrix} -1 & +1 \\ -1 & +1 \end{pmatrix} \tag{9}$$

$$K^e = \nu \int_{\Omega^e} \begin{pmatrix} \dfrac{\partial N_1}{\partial x} \dfrac{\partial N_1}{\partial x} & \dfrac{\partial N_1}{\partial x} \dfrac{\partial N_2}{\partial x} \\ \dfrac{\partial N_2}{\partial x} \dfrac{\partial N_1}{\partial x} & \dfrac{\partial N_2}{\partial x} \dfrac{\partial N_2}{\partial x} \end{pmatrix} dx = \frac{\nu}{h} \begin{pmatrix} +1 & -1 \\ -1 & +1 \end{pmatrix} \tag{10}$$

$$f^e = \int_{\Omega^e} \begin{pmatrix} N_1 \\ N_2 \end{pmatrix} dx = \frac{h}{2} \begin{pmatrix} +1 \\ +1 \end{pmatrix}. \tag{11}$$

Assembling the global system matrix, we obtain:

$$
\left\{
\begin{pmatrix}
-\dfrac{a}{2} + \cdots & \dfrac{a}{2} & \cdots \\
-\dfrac{a}{2} & \dfrac{a}{2} - \dfrac{a}{2} & \dfrac{a}{2} \\
\cdots & -\dfrac{a}{2} & \dfrac{a}{2} + \cdots
\end{pmatrix}
+
\begin{pmatrix}
\dfrac{\nu}{h} + \cdots & -\dfrac{\nu}{h} & \cdots \\
-\dfrac{\nu}{h} & \dfrac{\nu}{h} + \dfrac{\nu}{h} & -\dfrac{\nu}{h} \\
\cdots & -\dfrac{\nu}{h} & \dfrac{\nu}{h} + \cdots
\end{pmatrix}
\right\}
\begin{pmatrix} c_{j-1} \\ c_j \\ c_{j+1} \end{pmatrix}
=
\begin{pmatrix}
\dfrac{h}{2} + \cdots \\
\dfrac{h}{2} + \dfrac{h}{2} \\
\dfrac{h}{2} + \cdots
\end{pmatrix}.
\tag{12}
$$

The second row of the matrix is related to the coupled degrees of freedom at x_j and reads:

$$a\left(\frac{c_{j+1} - c_{j-1}}{2h}\right) - \nu\left(\frac{c_{j+1} - 2c_j + c_{j-1}}{h^2}\right) = 1. \tag{13}$$
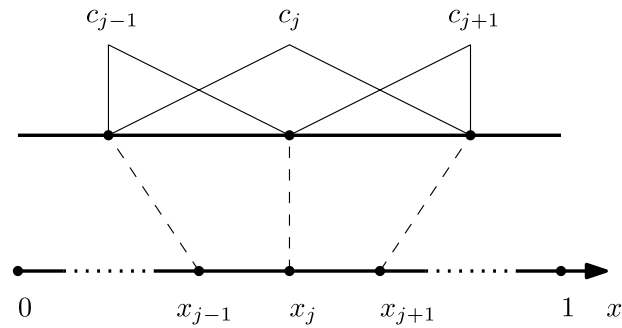
Fig. 1. 1D example with $p = 1$: three degrees of freedom in two elements.

By enforcing the exact solution in Eq. (2) at three adjacent nodes c_{j-1}, c_j and c_{j+1} and substituting the value in the differential equation [34], we obtain Eq. (14), which has a similar form to Eq. (13):

$$a\left(\frac{c_{j+1} - c_{j-1}}{2h}\right) - (\nu + \bar{\nu}_{ex})\left(\frac{c_{j+1} - 2c_j + c_{j-1}}{h^2}\right) = 1 \tag{14}$$

where $\bar{\nu}_{ex}$ is an extra term not present in Eq. (13). This extra term can be interpreted either as the truncation error of the first order Bubnov–Galerkin method or as an additional diffusivity required to provide nodally exact results. This term is a function of the *Péclet* number and reads:

$$\bar{\nu}_{ex} = \left(\coth(Pe) - \frac{1}{Pe}\right)\nu Pe. \tag{15}$$

Its value increases with the *Péclet* number. In fact, Eq. (15) forms the basic motivation behind using the streamline upwind Petrov–Galerkin method. In many stabilization approaches, one attempts to control the artificial numerical oscillations in convection dominated problems by compensating for the truncation error by adding extra diffusivity. As is shown in the next section, however, the truncation error of the Bubnov–Galerkin method is reduced simply by increasing the polynomial order of the spatial discretization.

4. Numerical diffusion in higher order finite element methods

This section looks at the same example as presented in Section 3. We first extend the analysis to the 2nd order whereby we use the concept of hierarchic shape functions derived from the set of integrated Legendre polynomials as introduced in [35]. In two dimensions, these shape functions can be classified into three groups: nodal or vertex modes, edge modes, and internal modes. The nodal or vertex modes are defined by the standard bilinear shape functions, familiar from the isoparametric four-noded quadrilateral element. Edge and internal modes are defined by tensor products of integrated Legendre polynomials. The edge modes are non-zero only on the edges with which they are associated and vanish on all other edges, whereas the internal modes are purely local, being zero on all vertices and edges of the quadrilateral element. In the simpler case of one dimension, we need only consider nodal and edge modes. In view of the following analysis, it is further remarked, that an increase in the order of approximation only leads to an addition of higher order modes while the lower order modes remain unchanged.

We now continue with the analysis of the one-dimensional case. The convection and stiffness matrices for $p = 2$ are computed as follows:

$$C^e = a \int_{\Omega^e} \begin{pmatrix} N_1 \dfrac{\partial N_1}{\partial x} & N_1 \dfrac{\partial N_2}{\partial x} & N_1 \dfrac{\partial N_3}{\partial x} \\ N_2 \dfrac{\partial N_1}{\partial x} & N_2 \dfrac{\partial N_2}{\partial x} & N_2 \dfrac{\partial N_3}{\partial x} \\ N_3 \dfrac{\partial N_1}{\partial x} & N_3 \dfrac{\partial N_2}{\partial x} & N_3 \dfrac{\partial N_3}{\partial x} \end{pmatrix} dx = \frac{a}{2} \begin{pmatrix} -1 & +1 & -\dfrac{\sqrt{6}}{3} \\ -1 & +1 & \dfrac{\sqrt{6}}{3} \\ \dfrac{\sqrt{6}}{3} & -\dfrac{\sqrt{6}}{3} & 0 \end{pmatrix} \tag{16}$$

$$K^e = \nu \int_{\Omega^e} \begin{pmatrix} \dfrac{\partial N_1}{\partial x}\dfrac{\partial N_1}{\partial x} & \dfrac{\partial N_1}{\partial x}\dfrac{\partial N_2}{\partial x} & \dfrac{\partial N_1}{\partial x}\dfrac{\partial N_3}{\partial x} \\ \dfrac{\partial N_2}{\partial x}\dfrac{\partial N_1}{\partial x} & \dfrac{\partial N_2}{\partial x}\dfrac{\partial N_2}{\partial x} & \dfrac{\partial N_2}{\partial x}\dfrac{\partial N_3}{\partial x} \\ \dfrac{\partial N_3}{\partial x}\dfrac{\partial N_1}{\partial x} & \dfrac{\partial N_3}{\partial x}\dfrac{\partial N_2}{\partial x} & \dfrac{\partial N_3}{\partial x}\dfrac{\partial N_3}{\partial x} \end{pmatrix} dx = \frac{\nu}{h} \begin{pmatrix} +1 & -1 & 0 \\ -1 & +1 & 0 \\ 0 & 0 & +2 \end{pmatrix} \tag{17}$$
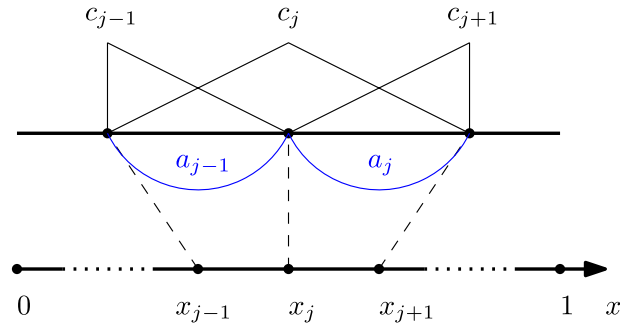
Fig. 2. 1D example with $p = 2$: five degrees of freedom in two elements.

$$f^e = \int_{\Omega^e} \begin{pmatrix} N_1 \\ N_2 \\ N_3 \end{pmatrix} dx = \frac{h}{2} \begin{pmatrix} +1 \\ +1 \\ -\frac{\sqrt{6}}{3} \end{pmatrix}. \tag{18}$$

The total number of degrees of freedom in two elements is five, consisting of three nodal modes and two internal modes, see Fig. 2.

It is worth noting that in one dimension the elements are only coupled by the linear modes. All higher order modes are purely local in terms of the element and thus independent from other degrees of freedom. One block of the global matrix, which corresponds to five degrees of freedom depicted in Fig. 2, is shown in Eq. (19).

$$\begin{array}{c} \phantom{c_{j-1}} \\ c_{j-1} \\ c_j \\ c_{j+1} \\ a_{j-1} \\ a_j \end{array} \begin{pmatrix} \frac{v}{h} - \frac{a}{2} + \cdots & -\frac{v}{h} + \frac{a}{2} + \cdots & & & -\frac{\sqrt{6}}{6}a \\ -\frac{v}{h} - \frac{a}{2} & \frac{2v}{h} & -\frac{v}{h} + \frac{a}{2} & \frac{\sqrt{6}}{6}a & -\frac{\sqrt{6}}{6}a \\ & -\frac{v}{h} - \frac{a}{2} + \cdots & \frac{v}{h} + \frac{a}{2} + \cdots & & \frac{\sqrt{6}}{6}a \\ \frac{\sqrt{6}}{6}a & -\frac{\sqrt{6}}{6}a & & \frac{2v}{h} & \\ & \frac{\sqrt{6}}{6}a & -\frac{\sqrt{6}}{6}a & & \frac{2v}{h} \end{pmatrix} \begin{pmatrix} c_{j-1} \\ c_j \\ c_{j+1} \\ a_{j-1} \\ a_j \end{pmatrix} = \begin{pmatrix} \frac{h}{2} + \cdots \\ h \\ \frac{h}{2} + \cdots \\ -\frac{\sqrt{6}}{6}h \\ -\frac{\sqrt{6}}{6}h \end{pmatrix}. \tag{19}$$

The discrete functions referring to degrees of freedom c_j, a_{j-1} and a_j can be computed independently. There are consequently three equations to solve:

$$\begin{cases} \frac{v}{h}(-c_{j-1} + 2c_j - c_{j+1}) + \frac{a}{2}\left(-c_{j-1} + \frac{\sqrt{6}}{3}(a_{j-1} - a_j) + c_{j+1}\right) = h \\ \frac{2v}{h}a_{j-1} + \frac{\sqrt{6}}{6}a(c_{j-1} - c_j) = -\frac{\sqrt{6}}{6}h \\ \frac{2v}{h}a_j + \frac{\sqrt{6}}{6}a(c_j - c_{j+1}) = -\frac{\sqrt{6}}{6}h \end{cases} \tag{20}$$

a_{j-1} and a_j, the variables related to the internal mode, can be eliminated from the last two equations. Substituting these variables into the first equation in Eq. (20), we arrive at the condensed Eq. (21), which is solely related to nodal degrees of freedom:

$$a\left(\frac{c_{j+1} - c_{j-1}}{2h}\right) - (v + \bar{v}_2)\left(\frac{c_{j+1} - 2c_j + c_{j-1}}{h^2}\right) = 1 \tag{21}$$

where

$$\bar{v}_2 = \frac{1}{3}Pe^2 v \tag{22}$$

$\bar{v}_2$ represents the additional numerical diffusion generated naturally[1] by the 2nd order Bubnov–Galerkin method of second order and can be regarded as an approximation to Eq. (15). Generally speaking, the system equation using polynomial

---

[1] 'Naturally' here means that this is the diffusion modeled by a pure *p*-extension. It does not stem from a method explicitly designed for stabilization by the 'artificial' addition of *extra* bubbles, as in the Residual-Free Bubble method [20–22].
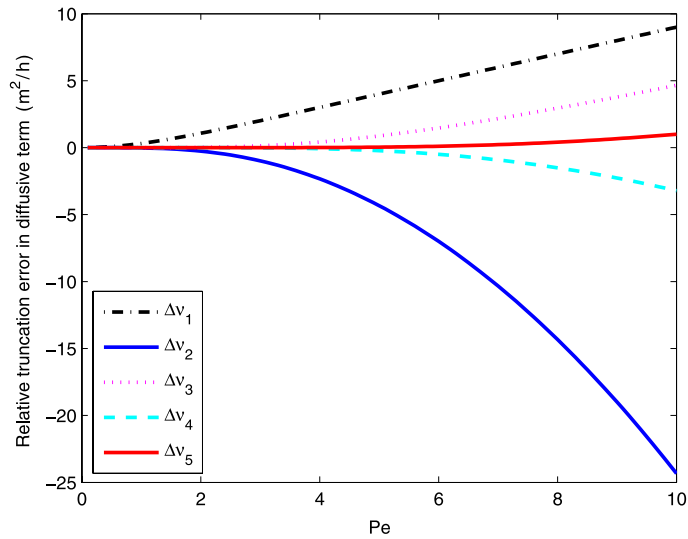
Fig. 3. Truncation error with different polynomial degrees.

degrees higher than 2 can also be similarly condensed in Eq. (23), as all higher modes are purely internal to the element. The resulting equation at node x_j is similar in form to Eq. (21):

$$a \left(\frac{c_{j+1} - c_{j-1}}{2h} \right) - (\nu + \bar{\nu}_p) \left(\frac{c_{j+1} - 2c_j + c_{j-1}}{h^2} \right) = 1. \tag{23}$$

The additional numerical diffusion term $\bar{\nu}_p$ can be computed in the same way. For the third, fourth and fifth order it reads:

$$\begin{aligned}
\bar{\nu}_3 &= \frac{5Pe^2 \nu}{Pe^2 + 15} \\
\bar{\nu}_4 &= \frac{\nu(Pe^4 + 35Pe^2)}{10Pe^2 + 105} \\
\bar{\nu}_5 &= \frac{14\nu(4Pe^4 + 90Pe^2)}{4Pe^4 + 420Pe^2 + 3780}.
\end{aligned} \tag{24}$$

In fact, the condensation approach from Eqs. (20) to (21) can be interpreted as follows: the contribution of the internal degrees of freedom in p-FEM is transferred to the contribution of nodal degrees of freedom located at the vertices of the element only. The solutions for the condensed system in Eq. (23), which consists solely of nodal degrees of freedom, are identical to the nodal solutions for the complete system, where the internal modes are also taken into account.

Compared to Eq. (15), the truncation error of p-FEM is defined as

$$\Delta \nu_p = \bar{\nu}_{ex} - \bar{\nu}_p \tag{25}$$

and depicted in dependence of Pe in Fig. 3, where the ordinate displays $\Delta \nu_p$. The curves generally have different tendencies which correspond to the parity of the polynomial degree. Odd degrees generate curves that increase monotonically as Pe increases, while the even ones decrease. Although the sign of the truncation error depends on the parity of the order, the absolute value of the truncation error decreases as the order of shape functions grows. Accordingly, the numerical solution at the nodes is closer to the exact solution.

On the other hand, using odd polynomial degrees, the numerical diffusivity of the high order approach is less than $\bar{\nu}_{ex}$. This lack of diffusivity is the reason for the oscillatory behavior of the numerical solution at high Pe. By contrast, the numerical diffusivity is always greater than $\bar{\nu}_{ex}$ using even polynomial degrees. Consequently, nodal solutions exhibit an over-diffusive behavior and never display nodal oscillations. This result is analyzed at greater depth from a mathematical perspective in the next section.

5. Stability analysis of nodal solutions

As the previous section has shown, the high order approach can diminish the numerical oscillations at nodes by recovering compensation for the lost diffusion of low order schemes. In this section, an eigenvalue analysis sets specific limits to the stability range according to the polynomial degree of the shape functions. We note that stability is evaluated solely at the nodal degrees of freedom and not for internal ones.

Table 1
Sharp stability bounds.

$p = 3$	$Pe = 2.322185$
$p = 5$	$Pe = 3.646738$
$p = 7$	$Pe = 4.971786$
$p = 9$	$Pe = 6.297019$
$p = 11$	$Pe = 7.622340$

It is a well-known fact (see [36]), for example, that a tridiagonal matrix **A**, as defined by

$$\mathbf{A}_{\text{alpha}} = \text{tridiag}(-1 - \alpha, 2, -1 + \alpha) \tag{26}$$

only has real eigenvalues if $\alpha \in [0, 1)$. Using linear elements in a Bubnov–Galerkin discretization for the convection–diffusion problem, the system matrix derived from Eq. (13) reads

$$\mathbf{A} = \frac{\nu}{h^2} \text{tridiag}(-1 - Pe, 2, -1 + Pe), \tag{27}$$

showing the direct correspondence between the *Péclet* number Pe and α. In the case of hierarchical higher order elements, the equations of internal degrees of freedom can be condensed out so that the system matrix contains only the equations of nodal degrees of freedom. Eq. (23) can be rewritten as

$$\left(-\frac{a}{2h} - \frac{(\nu + \bar{\nu}_p)}{h^2}\right) \cdot c_{j-1} + \frac{2(\nu + \bar{\nu}_p)}{h^2} \cdot c_j + \left(\frac{a}{2h} - \frac{(\nu + \bar{\nu}_p)}{h^2}\right) \cdot c_{j+1} = 1. \tag{28}$$

For the sake of clarity, we take the common factor $\frac{(\nu + \bar{\nu}_p)}{h^2}$ out of the brackets. The condensed system now has the same structure as Eq. (26).

$$\mathbf{A}_p = \frac{(\nu + \bar{\nu}_p)}{h^2} \text{tridiag}(-1 - \alpha_p, 2, -1 + \alpha_p)$$
$$\alpha_p = \frac{ah}{2(\nu + \bar{\nu}_p)}. \tag{29}$$

The stability of nodal solutions is accordingly determined by the value of α_p. It is, moreover, possible to quantify the value of α_p for higher order polynomial degrees based on Eqs. (22) and (24):

$$
\begin{aligned}
p = 2 \quad &\alpha_2 = \frac{3Pe}{Pe^2 + 3} \\
p = 3 \quad &\alpha_3 = \frac{Pe(Pe^2 + 15)}{6Pe^2 + 15} \\
p = 4 \quad &\alpha_4 = \frac{5Pe(2Pe^2 + 21)}{Pe^4 + 45Pe^2 + 105} \\
p = 5 \quad &\alpha_5 = \frac{Pe(Pe^4 + 105Pe^2 + 945)}{15(Pe^4 + 28Pe^2 + 63)} \\
p = 6 \quad &\alpha_6 = \frac{21Pe(Pe^4 + 60Pe^2 + 495)}{Pe^6 + 210Pe^4 + 4725Pe^2 + 10395} \\
p = 7 \quad &\alpha_7 = \frac{Pe(Pe^6 + 378Pe^4 + 17325Pe^2 + 135135)}{7(4Pe^6 + 450Pe^4 + 8910Pe^2 + 19035)}.
\end{aligned}
\tag{30}
$$

The corresponding values are plotted in Fig. 4. It can be observed that α_p increases as Pe for odd polynomial degrees. For even polynomial degrees, α_p first increases and then decreases, while the value always remains smaller than 1. This in turn means that the numerical solution never oscillates at nodal degrees of freedom for even polynomial degrees. This result also coincides with the conclusion from the truncation error analysis in the previous section. To clarify this point further, we plot the solution of the 1D example with $Pe = 20$, as shown in Fig. 5.

Fig. 5 illustrates that, when the polynomial degree is even, numerical oscillations only stem from internal modes and numerical solutions do not oscillate at each node. For odd polynomial degrees, numerical oscillations are reflected by both internal and nodal degrees of freedom.

By setting $\alpha_p = 1$ in Eq. (30), we are able to compute the highest Pe allowed, which guarantees nodally stable solutions for the given polynomial degree of the shape functions.

In other words, the corresponding p stated in Table 1 is the minimum polynomial degree required for a given *Péclet* number, and their relationship is depicted in Fig. 6. It turns out to be almost linear for polynomial orders $p \leq 11$. This result
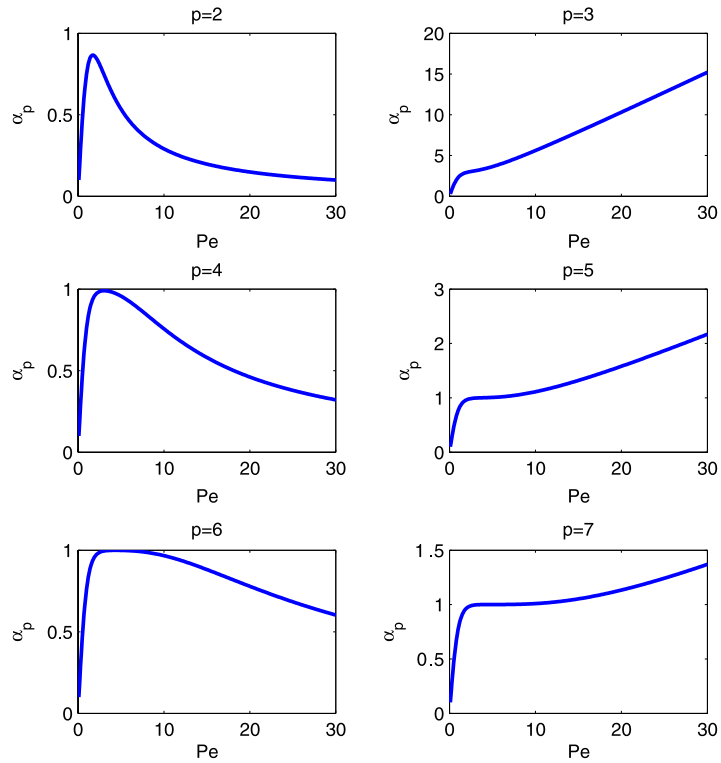
Fig. 4. α_p behaves differently for odd and even polynomial degrees.
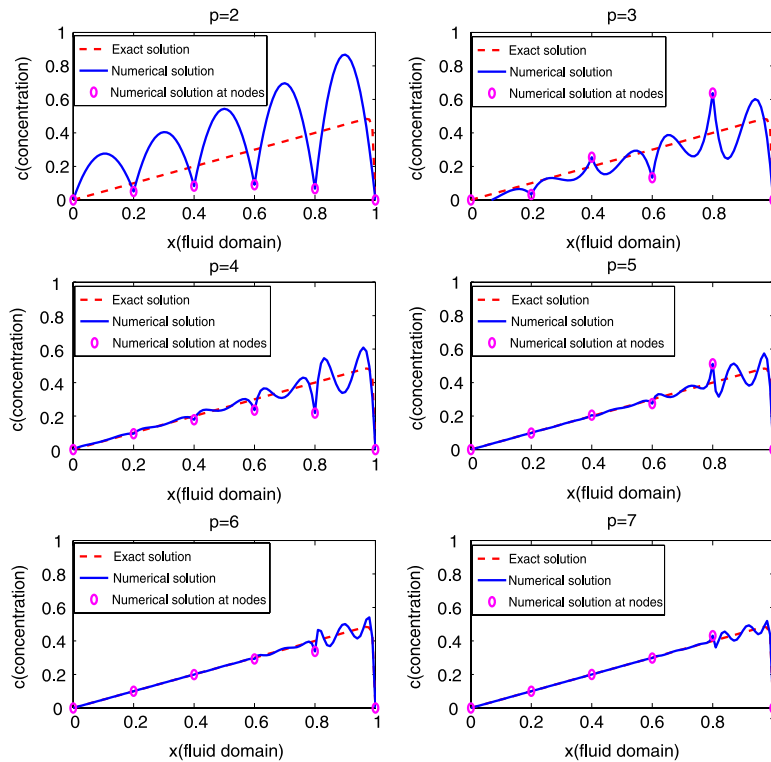

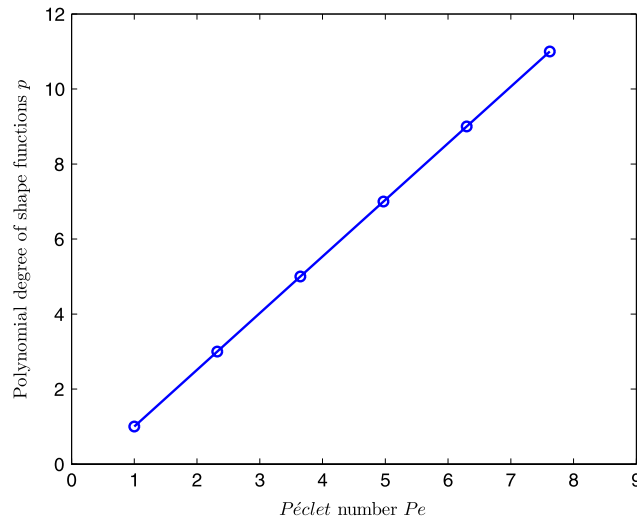**Fig. 5.** Numerical solutions with different Ansatz degree, $Pe = 20$.

Fig. 6. The relation between a given *Péclet* number and the minimum required polynomial degree.
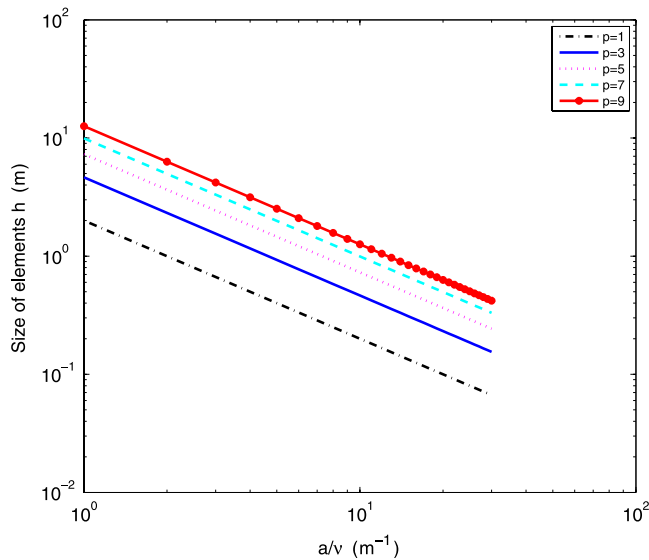

Fig. 7. The maximum mesh size allowed with respect to a/ν for different polynomial degrees.

agrees well with the estimate published in [32], where exponential convergence is achieved under a pure *p*-extension iff $\frac{ha}{\nu p}$ is of order 1. The value of the *Péclet* number includes the information of the element size *h*, so Table 1 also contains the relation between mesh size *h* and the polynomial degree *p* for a given $\frac{a}{\nu}$. The maximum mesh size allowed with respect to the value of $\frac{a}{\nu}$ is plotted for different orders in Fig. 7.

6. Numerical examples

6.1. One-dimensional convection–diffusion problem

In this example, the numerical result of the one-dimensional convection–diffusion transport problem is compared with the exact solution to verify the *Péclet* numbers stated in Table 1. We again consider the 1D convection–diffusion equation:

$$ac'(x) - \nu c''(x) = 1 \tag{31}$$

where the boundary condition is $c(x = 0) = c(x = 1) = 0$ in the domain $\Omega = (0, 1)$. We choose the parameters $a = 1.2$ m/h, $\nu = 0.02$ m^2/h, and compute the corresponding numerical solutions with 10 elements of the same length $h = 0.1$. The Bubnov–Galerkin method using linear elements produces the expected oscillations, since the *Péclet* number
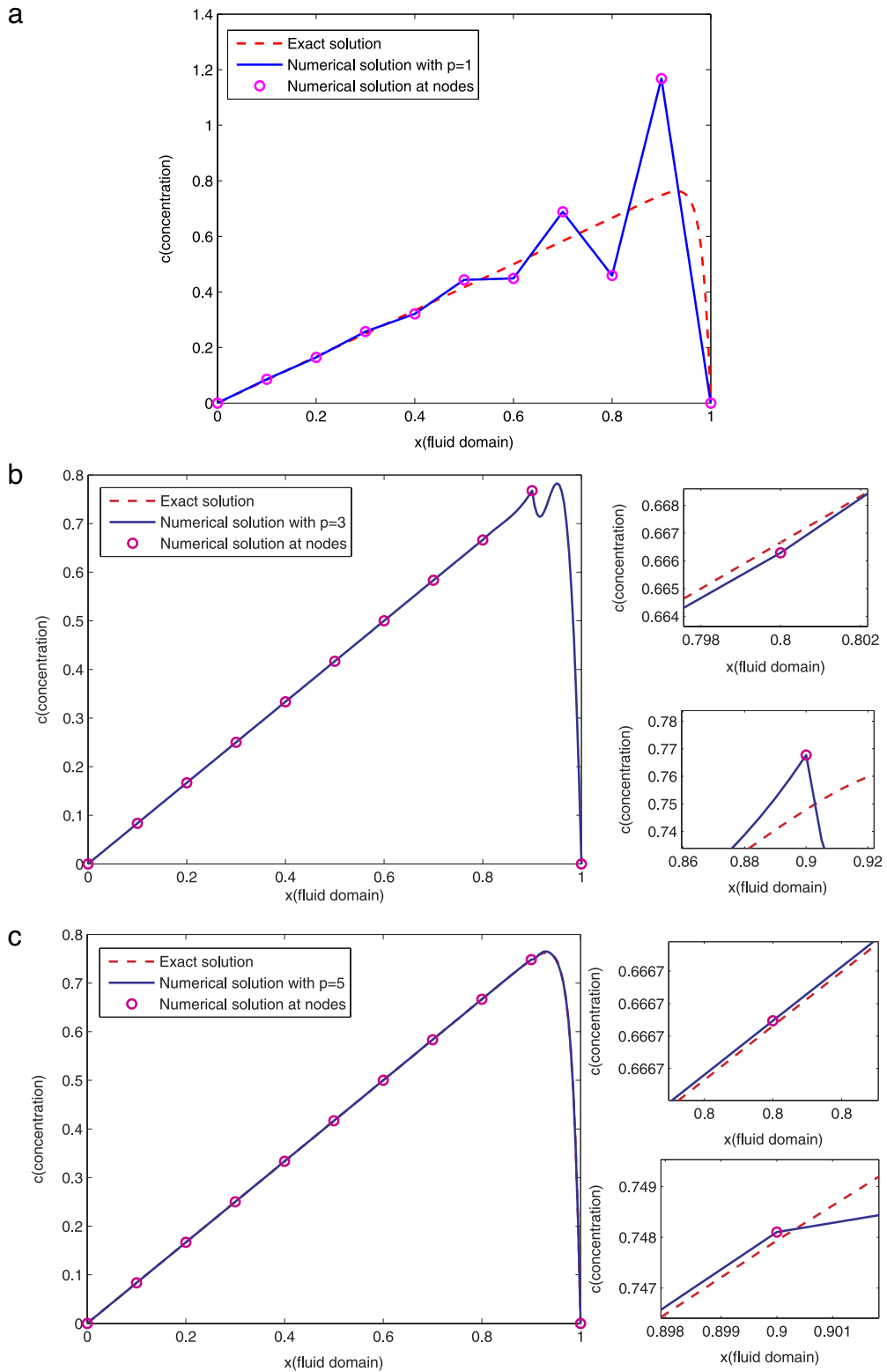
Fig. 8. The comparison of the numerical and exact solution with different polynomial degrees.

$Pe = \frac{ah}{2\nu} = 3$ is greater than 1. Fig. 8 shows the comparison between the exact solution and the numerical solution for different polynomial degrees.
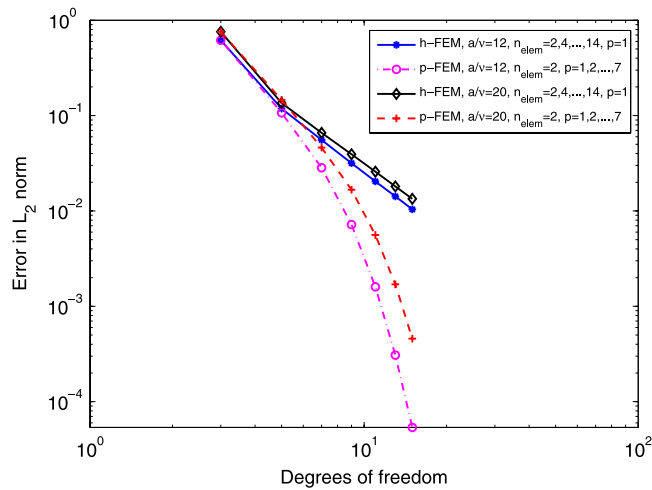
Fig. 9. Error in L_2 norm with different *Péclet* numbers.

The oscillations tend to decrease as the polynomial degree increases. Although the numerical oscillations with linear elements are considerably improved when we choose $p = 3$, the nodal solution still oscillates. The solution at node $x = 0.8$ is smaller than the exact solution, whereas the one at its neighboring node $x = 0.9$ is larger. With $p = 5$, the numerical solutions at both nodes are bigger than the exact solution, which shows straight away that the nodal oscillation has now vanished completely. This observation coincides perfectly with the results obtained mathematically which are collected in Table 1 in Section 5.

With a stabilized solution, it is now possible to enjoy the benefits of the exponential convergence rate of the *p*-version of the finite element method. The numerical error in the finite element approximation can be quantified by the error in the L_2 norm defined by:

$$\|e\|_{L_2}^2 = \int_\Omega e^2 d\Omega = \int_\Omega (c_{ex} - c_{fe})^2 d\Omega. \tag{32}$$

The result is plotted in Fig. 9 with a logarithmic scale, showing the convergence rate of the error in the L_2 norm by a pure *h*- and *p*-extension respectively. With different values of a/ν, the *p*-extension exhibits exponential convergence, whereas the *h*-extension only obtains an algebraic rate of convergence. This agrees very well with the results published in [32], according to which the order of the convergence for a pure *h*-extension in the energy norm should be $O\left(N^{-1/2}\right)$. We achieve double that rate in L_2. In addition, the effect of a/ν can also be observed in Fig. 7. If $(a/\nu, h)$ is located under any curve in Fig. 7, the nodally stable solution of the system for the corresponding polynomial degree p can be guaranteed.

6.2. Two-dimensional steady rotating pulse problem

Here, the stabilization of the Bubnov–Galerkin finite elements for high order shape functions is demonstrated on a two-dimensional diffusion–convection–reaction transport problem with a rotating velocity and a discontinuous source. The well-known partial differential equation reads:

$$a \cdot \nabla c - \nabla \cdot (\nu \nabla c) + \sigma c = f \tag{33}$$

where σ is the reaction coefficient. We apply the following boundary conditions $c(x = -1) = c(x = 1) = c(y = -1) = c(y = 1) = 0$ in the domain $\Omega = (-1, 1) \times (-1, 1)$. The velocity field is given as

$$a = \phi(\rho) \begin{pmatrix} -y \\ x \end{pmatrix} \tag{34}$$

where

$$\begin{cases} \phi(\rho) = \begin{cases} 1 - \rho^2 & \text{if } \rho \leq 1 \\ 0 & \text{else} \end{cases} \\ \rho = \sqrt{x^2 + y^2}. \end{cases} \tag{35}$$

For the following computations, the coefficients are defined as $\sigma = 2$, $\nu = 0.0001$ and the source term is:

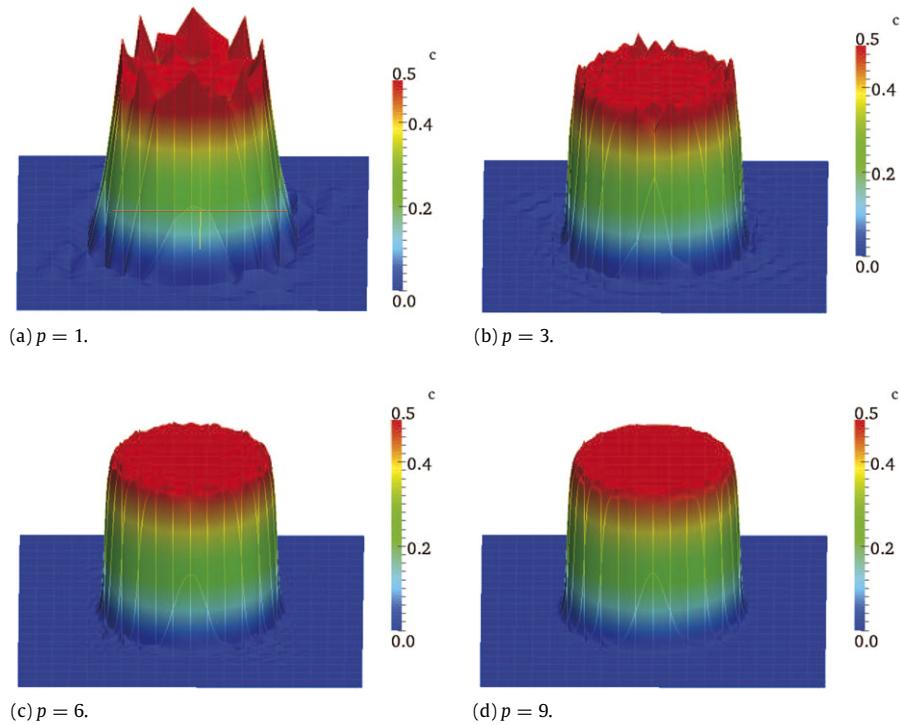$$f = \begin{cases} 1 & \text{if } \rho \leq 1/2 \\ 0 & \text{else.} \end{cases} \tag{36}$$

(a) $p = 1$.   (b) $p = 3$.

(c) $p = 6$.   (d) $p = 9$.

Fig. 10. Two-dimensional steady rotating pulse problem: The numerical solutions with different polynomial degrees.
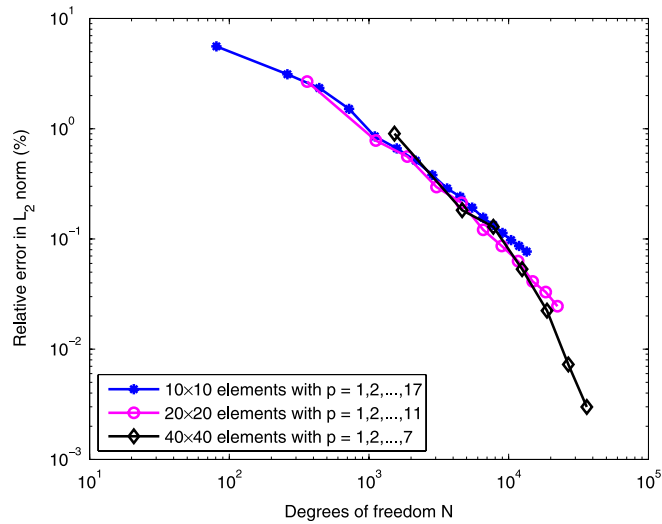

Fig. 11. Two-dimensional steady rotating pulse problem: Error in L_2 norm with different *Péclet* numbers.

This example is also discussed in [34]. The result has a front layer along the circle $\rho = 1/2$. In this case, a uniform mesh with 20×20 elements is applied and the numerical solution based on different polynomial degrees of shape functions is depicted in Fig. 10.

The numerical result exhibits a strong oscillation along the front with the application of linear elements. This numerical oscillation is drastically reduced or even suppressed by increasing the polynomial degree, as shown in Fig. 10. The convergence for different meshes and polynomial degrees is depicted in Fig. 11.

7. Conclusion and outlook

This paper investigates the Bubnov–Galerkin method for convection–diffusion problems. It leads to numerical oscillations for convection-dominated problems where *low* order finite elements are employed. This treatise demonstrates, however,

that it is possible to achieve nodally stable solutions for a given *Péclet* number greater than 1 by increasing the degree of the shape functions. The polynomial degree required for a certain *Péclet* number is analytically derived in this paper. Numerical examples verify these theoretical findings.

A high-order discretization does not only provide numerical stability. Numerical examples show that the solution converges exponentially when the polynomial degree is increased. This observation forms the basic motivation for using standard Bubnov–Galerkin finite elements with a *p*-extension for problems connected with multi-component flow, etc. Moreover, this result is especially important for applying the method in simulations of ground water flow through highly heterogeneous media, where only moderate *Péclet* numbers appear. This is subject to current research, see [37,38], for instance, for an extension of the findings of this paper to include the finite cell method, a combination of high order finite elements and a fictitious domain method.

Acknowledgments

References

[1] A. Brooks, T. Hughes, Streamline upwind Petrov–Galerkin formulations for convection dominated flows with particular emphasis on the incompressible Navier–Stokes equations, Computer Methods in Applied Mechanics and Engineering 32 (1982) 199–259.
[2] T. Hughes, L. Franca, M. Mallet, A new finite element formulation for computational fluid dynamics: I. Symmetric forms of the compressible Euler and Navier–Stokes equations and the second law of thermodynamics, Computer Methods in Applied Mechanics and Engineering 54 (1986) 223–234.
[3] M. Braack, E. Burman, Local projection stabilization for the oseen problem and its interpretation as a variational multiscale method, SIAM Journal on Numerical Analysis 43 (2006) 2544–2566.
[4] G. Matthies, P. Skrzypacz, L. Tobiska, Stabilization of local projection type applied to convection–diffusion problems with mixed boundary conditions, Electronic Transactions on Numerical Analysis 32 (2006) 90–105.
[5] P. Knobloch, L. Tobiska, On the stability of finite-element discretizations of convection–diffusion–reaction equations, IMA Journal of Numerical Analysis 31 (2011) 147–164.
[6] R. Codina, J. Blasco, Analysis of a stabilized finite element approximation of the transient convection–diffusion–reaction equation using orthogonal subscales, Computing and Visualization in Science 4 (2002) 167–174.
[7] I. Harari, T.J.R. Hughes, Stabilized finite element methods for steady advection–diffusion with production, Computer Methods in Applied Mechanics and Engineering 115 (1994) 165–191.
[8] T.J.R. Hughes, Multiscale phenomena: Green's functions, the Dirichlet-to-Neumann formulation, subgrid scale models, bubbles and the origins of stabilized methods, Computer Methods in Applied Mechanics and Engineering 127 (1995) 387–401.
[9] T.J.R. Hughes, G.M. Hulbert, Large eddy simulation and the variational multiscale method, Computing and Visualization in Science 3 (2000) 47–59.
[10] T.J.R. Hughes, G. Sangalli, Variational multiscale analysis: the final-scale Green's functions, projection, optimization, localization and stabilized methods, SIAM Journal on Numerical Analysis 45 (2007) 539–557.
[11] A. Quarteroni, Numerical Models for Differential Problems, Springer-Verlag, 2009.
[12] E. Burman, A. Quarteroni, B. Stamm, Stabilization strategies for high order methods for transport dominated problems, Bollettino della Unione Matematica Italiana. Serie 9 1 (2008) 57–77.
[13] J.S. Hesthaven, T. Warburton, Nodal Discontinuous Galerkin Methods, Springer-Verlag, 2008.
[14] L. Demkowicz, J. Gopalakrishnan, A class of discontinuous Petrov–Galerkin methods. Part I: The transport equation, Computer Methods in Applied Mechanics and Engineering 199 (2010) 1558–1572.
[15] L. Demkowicz, J. Gopalakrishnan, A class of discontinuous Petrov–Galerkin methods. Part II: Optimal test functions, Numerical Methods for Partial Differential Equations 27 (2011) 70–105.
[16] J. Zitelli, I. Muga, L. Demkowicz, J. Gopalakrishnan, D. Pardo, V. Calo, A class of discontinuous Petrov–Galerkin methods. Part IV: Wage propagation problems, Journal of Computational Physics 230 (2011) 2406–2432.
[17] L. Demkowicz, J. Gopalakrishnan, A. Niemi, A class of discontinuous Petrov–Galerkin methods. Part III: Adaptivity, Applied Numerical Mathematics 62 (2012).
[18] P. Bochev, K. Peterson, A parameter-free stabilized finite element method for scalar advection–diffusion problems, Central European Journal of Mathematics (2012) 1–18.
[19] J. Evans, T. Hughes, G. Sangalli, Enforcement of constraints and maximum principles in the variational multiscale method, Computer Methods in Applied Mechanics and Engineering 199 (2009) 61–76.
[20] F. Brezzi, A. Russo, Choosing bubbles for advection–diffusion problems, Mathematical Models and Methods in Applied Sciences 4 (1994) 571–587.
[21] C. Canuto, Stabilization of spectral methods by finite element bubble functions, Computer Methods in Applied Mechanics and Engineering 116 (1994) 13–26.
[22] A. Russo, Bubble stabilization of the finite element methods for the linearized incompressible Navier–Stokes equation, Computer Methods in Applied Mechanics and Engineering 132 (1996) 335–343.
[23] C. Canuto, G. Puppo, Bubble stabilization of spectral Legendre methods for the advection–diffusion equation, Computer Methods in Applied Mechanics and Engineering 118 (1994) 239–263.
[24] F. Brezzi, T.J.R. Hughes, L. Marini, A. Russo, E. Sli, A priori error analysis of residual-free bubbles for advection–diffusion problems, SIAM Journal on Numerical Analysis 36 (1999) 1933–1948.
[25] G. Sangalli, Global and local error analysis for the residual-free bubbles method applied to advection-dominated problems, SIAM Journal on Numerical Analysis 38 (2000) 1496–1522.
[26] F. Brezzi, G. Hauke, L. Marini, G. Sangalli, Link-cutting bubbles for convection–diffusion–reaction problems, Mathematical Models and Methods in Applied Sciences 3 (2003).
[27] F. Brezzi, L. Franca, T. Hughes, A. Russo, $b = \int g$, Computer Methods in Applied Mechanics and Engineering 145 (1997) 329–339.
[28] L. Tobiska, Analysis of a new stabilized higher order finite element method for advection–diffusion equations, Computer Methods in Applied Mechanics and Engineering 196 (2006) 538–550.
[29] H.-G. Roos, M. Stynes, L. Tobiska, Robust Numerical Methods for Singularly Perturbed Differential Equations, in: Springer Series in Computational Mathematics, vol. 24, 2008.
[30] G. Lube, G. Rapin, Residual-based stabilized higher-order FEM for advection-dominated problems, Computer Methods in Applied Mechanics and Engineering 195 (2006) 4124–4138.

[31] C. Canuto, M.Y. Hussaini, A. Quateroni, T. Zank, Spectral Methods in Fluid Dynamics, Springer-Verlag, New York, 1993.
[32] C. Schwab, M. Suri, C. Xenophontos, Boundary layer approximation by spectral/*hp* methods, Houston Journal of Mathematics (1996) 501–508. Special Issue of ICOSAHOM'95 Conference.
[33] C. Schwab, M. Suri, The *p* and *hp* versions of the finite element method for problems with boundary layers, Mathematics of Computation 65 (1996) 1403–1429.
[34] J. Donea, A. Huerta, Finite Element Methods for Flow Problems, John Wiley & Sons, 2003.
[35] B. Szabó, I. Babuška, Finite Element Analysis, John Wiley & Sons, 1991.
[36] O. Ernst, Residual-minimizing Krylov subspace methods for stabilized discretization of convection–diffusion equations, SIAM Journal on Matrix Analysis and Applications 21 (2000) 1079–1101.
[37] Q. Cai, S. Kollmannsberger, R.-P. Mundani, E. Rank, The finite cell method for solute transport problems in porous media, in: 16th International Conference on Finite Elements in Flow Problems.
[38] Q. Cai, S. Kooshapur, M. Manhart, R.-P. Mundani, E. Rank, Numerical simulation of transport in porous media: some problems from micro to macro scale, in: M. Baader, H. Bungartz, T. Weinzierl (Eds.), Advanced Computing, in: Lecture Notes in Computational Science and Engineering, Springer, 2013, in press.